Electron Acceptability of Cyclopenta-Fused Polycyclic Aromatic Hydrocarbons: Effect of One Electron

Pamela C. Ubaldo, Nathan D. Colley, Kyle N. Plunkett, and Lichang Wang*

Department of Chemistry and Biochemistry and the Materials Technology Center, Southern Illinois University, Carbondale, IL 62901, United States

ABSTRACT

To accurately predict the electron acceptability of cyclopenta-fused polycyclic aromatic hydrocarbons (CP-PAHs), we evaluated the performance of six functionals, B3LYP, CAM-B3LYP, HSEH1PBE, PBE, TPSS, and HCTH, using eight CP-PAHs. The results show that B3LYP is the best to obtain the energy of the highest occupied molecular orbital (HOMO), the energy of the lowest unoccupied molecular orbital (LUMO), and the HOMO-LUMO energy gap of CP-PAHs with a mean absolute error (MAE) of 0.14 eV. The current study also demonstrates that calculations must be carried out for the anion of the corresponding CP-PAH in order to predict LUMO energy of an electron acceptor. Time-dependent CAM-B3LYP with the B3LYP optimized geometry predicts the absorption spectra of CP-PAHs most accurately with a MAE of 29 nm. The results from B3LYP and time-dependent CAM-B3LYP calculations coupled with the new practice in calculating LUMO energy presented in this work show that six of the eight CP-PAHs can accept electrons from the donor material poly(3-hexylthiophene)(P3HT), thus indicating they can be used as electron acceptors of P3HT. Moreover, three pairs of CP-PAHs were identified for their use as highly efficient organic solar cell materials through construction of a P3HT-acceptor1-acceptor2 architecture.

1. Introduction

Research on rational design of solar cells has continued to garner significant attention and has made considerable progress in developing sustainable photovoltaic technology.[1-12] To improve the efficiency of organic photovoltaic (OPV) cells, various new design strategies have recently been developed.[13-28] For example, Cnops *et al.* improved the small-molecule OPV efficiencies to 8.5% by exploiting long-range exciton energy transfer.[13] We recently demonstrated efficiency improvements in OPVs that incorporate two electron acceptors to form a cascading donor-acceptor1-acceptor2 architecture[14, 29] as well as charge-separated sensitizers.[12, 23, 30-34] In the evaluation of these architectures, it became apparent that intimate knowledge of the frontier orbitals energies, via experiment as well as calculation, of the acceptor is invaluable. We recently developed a new class of functionalizable cyclopenta-fused polycyclic aromatic hydrocarbons (CP-PAHs) that are efficient electron acceptors and have the potential to replace Buckminster fullerenes in OPVs.[15] These CP-PAHs have high electron affinity, can be used as electron transport materials, and are quite stable, which make them suitable n-type materials for organic field effect transistors and OPVs.[15, 35-41] In addition, these compounds have unusual photophysical properties, such as anomalous fluorescence[42-43] and absorption spectra that are strongly modulated by the arrangement and the number of cyclopentene rings present and therefore provide an interesting class of compounds to study computationally.[44]

Accurate prediction of the electronic properties and absorption spectra of CP-PAHs is important in the development of these compounds for their successful utilization in electronic devices. The use of computation in predicting electronic and optical properties of CP-PAHs is an essential step in the rational and directed design of new materials. Our previous B3LYP study of two CP-PAHs, 2,7-bis((4-(decycloxy)phenyl)ethynyl)cyclopenta[hi] aceanthrylene and 2,8-

bis((4-decycloxy)phenyl)ethynyl)dicyclopenta[de,mn]tetracene, predicted the energies of the highest occupied molecular orbital (HOMO) and the lowest unoccupied molecular orbit (LUMO) and the HOMO-LUMO energy gap (ΔE_{gap}) to be about 0.4 eV higher or larger than the experiment and λ_{max} about 150 nm longer than the experimental data.[15] A better prediction of HOMO energy, LUMO energy, ΔE_{gap}, and absorption spectra is necessary in order to effectively facilitate the translation of materials into devices such as OPVs.

Density Functional Theory (DFT) and Time Dependent DFT (TD-DFT) are widely used to calculate HOMO energy, LUMO energy, ΔE_{gap}, and absorption spectra of materials. The accuracy of these quantities is often dependent on the functional, basis set, and type of system being studied.[45] Becke's three-parameter exchange functional with the Lee-Yang-Parr correlation functional (B3LYP)[46-47] is most widely used in predicting HOMO, LUMO, ΔE_{gap}, and λ_{max} of a wide range of systems. However, B3LYP does not always provide the most accurate results.[48-49] Le Baher *et al.* studied properties of C, Si, Ge, CdO, CdS, CdSe, CdTe, GaAs, TiO_2, and ZnO semiconductors and found that HSE06 functional is the best in predicting ΔE_{gap} with a mean absolute error (MAE) of 0.21 eV, while B3LYP has a MAE of 0.56 eV.[50] A continuous quest toward improving the accuracy of HOMO, LUMO, and ΔE_{gap} prediction using DFT has been explored by several groups. Su and coworkers, in their study on fractional charge behavior and band gap prediction of Li, Be, B, C, N, O, F, F_2, OH, NH_2, CH_3 and CN, illustrated that XY3G, a doubly hybrid functional, with the cc-PVQZ basis set predicts ionization potential (HOMO), electron affinity (LUMO), and ΔE_{gap} with MAE of 0.10, 0.37, and 0.39 eV, respectively, whereas B3LYP gives MAE of 0.37, 0.25, and 0.59 eV, respectively.[51]

Zhang and Musgrave performed calculations for a set of twenty-seven molecules from H_2 to $C_{14}H_{10}$ and found KMLYP, BH&HLYP, and B3LYP are the top three (out of eleven) functionals for predicting HOMO with MAE of 0.73, 1.48, and 3.10 eV, respectively. The predicted ΔE_{gap} using KMLYP, BH&HLYP, B3LYP were 4.96, 4.29, and 1.63 eV, respectively. The predicted ΔE_{gap} using the GGA functionals were relatively accurate (~0.73 eV) despite the inaccuracy in predicting the HOMO and LUMO energy levels. All eleven functionals used in their study inaccurately predicted the LUMO level due to the poor description of the virtual orbitals that results from extensive relaxation of occupied orbitals.[52]

Efforts toward improving accuracy of TD-DFT calculations of absorption spectra and excited state energies are also ongoing. The choice of best functional for TD-DFT is dependent on both the excitation mechanism as well as the type of system being studied. Several groups have found a correlation between the excitation energy error and the overlap parameter (Λ) of the orbitals involved in excitation. An increase in excitation energy errors is found from the local excitation to the charge transfer excitation mechanism, which has decreasing Λ. CAM-B3LYP is found to perform best even for the systems with charge transfer mechanisms.[53-58] For example, Rabilloud found CAM-B3LYP and ωB97x are the two most accurate functionals in calculating absorption spectra and the lowest excitation energy of silver clusters (Ag_n) with MADs of 0.08 and 0.09 eV, respectively, for clusters with n= 4, 6, 8, 12, 18, and 20.[59] Guo *et al.* found CAM-B3LYP to predict absorption spectra of eight benzoic acid derivatives better than fourteen other functionals with the lowest MAE of 0.24 eV for thirty-seven excitation energies.[60]

This study aims to describe an accurate method in predicting the electronic properties and absorption spectra of CP-PAHs by establishing the best functional and an appropriate computational protocol. In this work, we chose six functionals, namely B3LYP, CAM-B3LYP, HSEH1PBE,[61-62] PBE,[63] TPSS,[64] and HCTH[65] to search for the most accurate functional for the HOMO, LUMO, ΔE_{gap}, and absorption spectra. Eight CP-PAHs shown in Figure 1 were used in the data set with **1** and **2** to build the improved computational protocol, while **3-8** were used for validation.

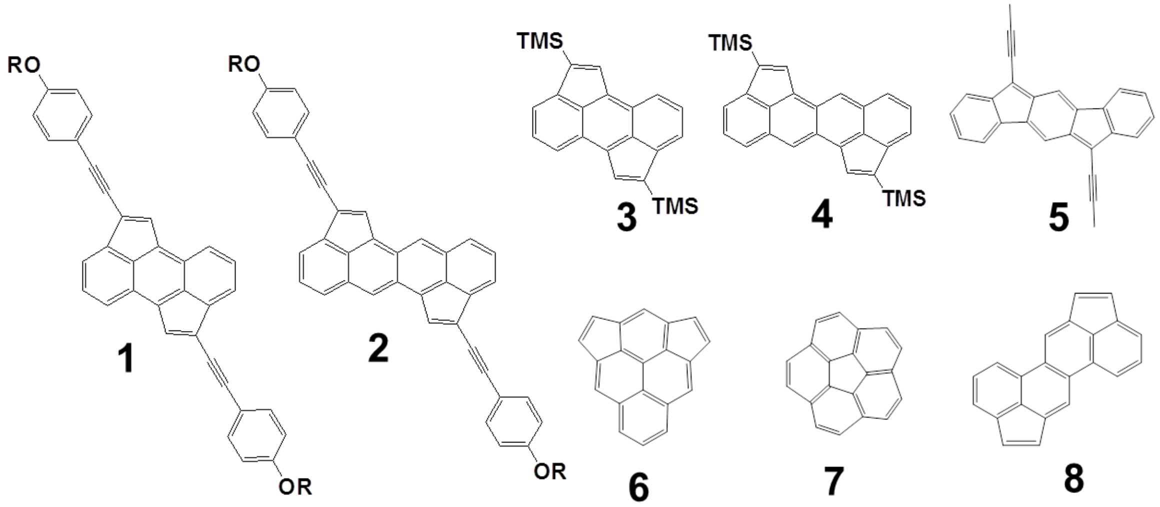

Figure 1. CP-PAH structures: 2,7-bis((4-(alkoxy-)phenyl)-ethynyl)cyclopenta[hi]aceanthrylene (**1**, R=H, CH_3, C_2H_5, $CH_2CH_2CH_3$); 2,8-bis((4-alkoxy-)phenyl)ethynyl)dicyclopenta[de,mn] tetracene (**2**); 2,7-bis (trimethylsilyl) cyclopenta[hi]aceanthrylene (**3**); 2,8-bis(trimethylsilyl) dicyclopenta[de,mn]tetracene (**4**); 6,12-diethynylindeno[1,2-b]fluorine (**5)**; dicyclopenta[cd,mn] pyrene (**6**); corannulene (**7**); dicyclopenta[hi,qr]chrysene (**8**).

2. Computational Details

All geometry optimizations, frequency calculations, and single-point energy calculations to obtain absorption spectra were carried out using Gaussian09 software.[66] For the convenience of further analysis, we provide in Table 1 a summary of the six functionals used in this work. The 6-311G(d,p) basis set was used in all of the calculations. Our previous work has shown that such a basis set is sufficient to ensure the accuracy of the results.[37, 67-68] The solvent used for **1-5** is tetrahydrofuran (THF) and **6-8** acetonitrile (CH_3CN) so that comparisons can be made with experiments. The solvents were treated using the polarized continuum model (PCM) for all calculations. **1** and **2** were used in the development of this protocol for predicting electronic properties and absorption spectra of CP-PAHs and for probing the effects of varying lengths of alkyl chains on functionalized CP-PAHs. **3-8** were used for validation of the method. All geometry optimizations followed convergence criteria for self-consistent field (SCF), gradient, and energy of 10^{-8}, 10^{-6}, and 10^{-6} a.u., respectively. Each geometry optimization was succeeded by a frequency calculation and probed for the absence of imaginary frequencies, ensuring the structure at an energetic minimum. TD-DFT calculations using twenty-four states were performed on the optimized structures to predict absorption spectra and obtain the information on electron excitation.

Table 1. E_{xc} formalism of the six functionals

Functional	Exchange Energy	Correlation Energy
B3LYP[46-47]	$0.2E_X^{HF} + 0.8E_x^{Slater} + 0.72\Delta E_x^{B88}$	$0.81E_c^{LYP} + 0.19E_c^{VWN}$
CAMB3LYP[69]	$0.19E_X^{HF} + 0.81E_x^{Slater} + 0.81\Delta E_x^{B88}$	$0.81E_c^{LYP} + 0.19E_c^{VWN}$
HSEH1PBE[61-62]	$0.25E_x^{SR-HF}(\omega) + 0.75E_x^{SR-PBE}(\omega) + E_x^{LR-PBE}(\omega)$	$\int d^3r\, n[\epsilon_c^{unif}(r_s, \zeta) + H(r_s, \zeta, t)]$
PBE[63]	$\int d^3r\, n\epsilon_x^{unif}(n)F_x(s)$	$\int d^3r\, n[\epsilon_c^{unif}(r_s, \zeta) + H(r_s, \zeta, t)]$
TPSS[64]	$\int d^3r\, n\epsilon_x^{unif}(n)F_x(p,z)$	$\int d^3r\, n\epsilon_c^{revPKZB}$ x $[1 + d\epsilon_c^{revPKZB}(\tau^W/\tau)^3]$
HCTH[65]	$\sum_\sigma \int e_{X\sigma}^{LSDA}(\rho_\sigma) g_{X\sigma}(s_\sigma^2)\,dr$	$\sum_\sigma E_{C\sigma\sigma} + E_{C\alpha\beta}$

3. Results and Discussion

The quantities to predict the feasibility of CP-PAHs as electron acceptors include the energies of HOMO and LUMO, ΔE_{gap}, and absorption spectra. As such, we compared the accuracy of these values obtained from different functionals with the corresponding experimental measurements and selected the best functional for the quantities of interest for CP-PAHs using 2 CP-PAH molecules, which is presented in section 3.1. To further verify our method, we tested 6 other CP-PAHs. The results are presented in section 3.2. Once the most accurate method was chosen, we studied the feasibility of these CP-PAHs as electron acceptors of the donor material poly(3-hexylthiophene)(P3HT) and the findings are presented in section 3.3.

3.1 The Best Protocol for Studying Electronic and Optical Properties of Electron Acceptors

3.1.1 Effects of –R Groups on the calculated properties of 1 and 2.

Experimentally synthesized **1** and **2** originally contain $C_{10}H_{21}$ as the –R groups. However, the theoretical model in our previous study used a truncated $–CH_3$ group to save computing time.[15] We expected that the important quantities for these compounds as electron acceptor, i.e. HOMO, LUMO, ΔE_{gap}, and absorption spectra, would not be affected based on our previous experience on other molecules[67] and by the inspection of the molecular orbitals of **1** and **2**. To give justice to the simplified models for **1** and **2**, the effects of different –R groups on the electronic properties and absorption spectra of **1** and **2** were investigated. We screened different –R groups including –H, $-CH_3$, $-C_2H_5$, and $-C_3H_7$. The calculated electronic properties of **1** and **2** with different –R groups are given in Table 2.

Table 2. Electronic properties (in eV) in THF of 1 and 2 with varying –R groups obtained from B3LYP/6-311G(d,p) calculations

	1			**2**		
-R	HOMO	LUMO	ΔE_{gap}	HOMO	LUMO	ΔE_{gap}
-H	-5.19	-3.31	1.88	-5.14	-3.32	1.82
$-CH_3$[a]	-5.18	-3.31	1.87	-5.13	-3.31	1.82
$-C_2H_5$	-5.17	-3.30	1.87	-5.12	-3.31	1.81
$-C_3H_7$	-5.17	-3.30	1.87	-5.12	-3.31	1.81

[a] Data taken from Ref. [15].

As expected, with increasing R group's chain length, the HOMO, LUMO and ΔE_{gap} remain very similar for the two CP-PAHs. The absence of significant electronic changes to the chromophore, **1** or **2**, as the length of alkyl chain is increased indicates the nature of alkyl chain does not influence the electronic properties of functionalized CP-PAHs. Thus, the replacement of long alkyl chains with $–CH_3$ in CP-PAHs is sufficient for modeling the electronic properties of alkyl functionalized CP-PAHs.

The effect of different –R groups on the absorption spectra of **1** and **2** was also probed by comparing the absorption spectra and the results are depicted in Figure 2. The change in alkyl chain length attached to **1** and **2** produced similar and almost overlapping absorption spectra. However, as the –R groups changed from –H to $–C_nH_{2n+1}$ with n=1-3, a small bathochromic shift was observed. As shown in Figure 2, the replacement of H in **1** and **2** by the three alkyl groups produced a red shift of about 5 nm. There are no apparent shifts among the spectra using three alkyl chains. These suggest that the model containing $–CH_3$ instead of the longer alkyl chain is sufficient for calculating absorption spectra of alkyl functionalized CP-PAHs. In essence, the results indicate one can replace an alkyl chain with $–CH_3$ in the calculations of electronic and absorption spectrum of a CP-PAH to save computing time as long as the alkyl chain is not involved in the HOMO and LUMO orbitals.

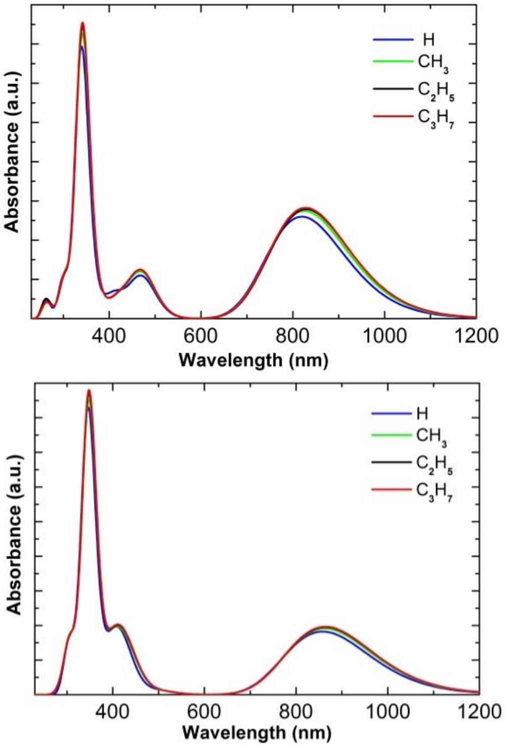

Figure 2. Absorption spectra of **1** (top) and **2** (bottom) with various –R groups in THF obtained from B3LYP/6-311G(d,p).

3.1.2. Changes in Electronic Properties of CP-PAHs When Accepting One Electron

The HOMO, LUMO, and ΔE_{gap} were conventionally obtained in DFT calculations of neutral CP-PAHs.[15] However, one needs to be cautious when comparing these values with experimental data. For example, the energy of the LUMO levels of CP-PAHs were measured electrochemically by adding an electron to the LUMO.[15] Comparing the calculated LUMO energy of a neutral species with the LUMO energy from an electrochemical measurement would indicate that we assume the LUMO energy of the compound remains unchanged upon accepting an electron. This assumption will undoubtedly result in a discrepancy between the experiment and computation in LUMO energy as well as ΔE_{gap} if the LUMO energy is changed substancially upon accepting an electron. A true comparison of LUMO energy should therefore be made by calculating the species with a negative charge.

As such, we performed calculations of both neutral **1** and the corresponding anion in -1 state to evaluate the amount of discrepancy arising from the use of data only from the neutral compound. Before we discuss the results on the electronic properties, we first present the changes on the bond distances when an electron is added to the neutral species. DFT results showed that, upon gaining an electron, the atomic bond distances in the cyclopenta[hi]aceanthrylene core change considerably. Eight out of the twenty two C-C bond lengths in this aromatic core decreased significantly with B3LYP, HSEH1PBE, PBE, TPSS, and HCTH calculations. However, when using CAM-B3LYP, ten out of twenty-two C-C bond lengths decreased significantly. More noticeably, adjacent C-C bonds present in the five-membered rings changed most significantly. The range of bond length changes that occurred in the cyclopenta[hi]aceanthrylene core of **1** is summarized in Table 3. Although the magnitude of changes in bond length can vary among different functional calculations, it is clear that significant changes will appear when the compound is reduced and we expect the corresponding electronic properties to be altered accordingly.

Table 3. Changes in C-C bond length (in Å) in the PAH core when 1 is reduced to 1$^-$.

Functional	Increase	Decrease
B3LYP	0.0003 – 0.0240	0.0128 – 0.0257
CAMB3LYP	0.0011 – 0.0283	0.0029 – 0.0347
HSEH1PBE	0.0004 – 0.0229	0.0121 –0.0242
PBE	0.0010 – 0.0179	0.0091 –0.0165
TPSS	0.0008 – 0.0195	0.0094 – 0.0184
HCTH	0.0009 – 0.0179	0.0092 – 0.0170

Contour plots and energy levels of **1** in the 0 and -1 state in Figure 3 provide a more clear view of electronic energy changes that occur in the experimental cyclic voltammetry.[4]

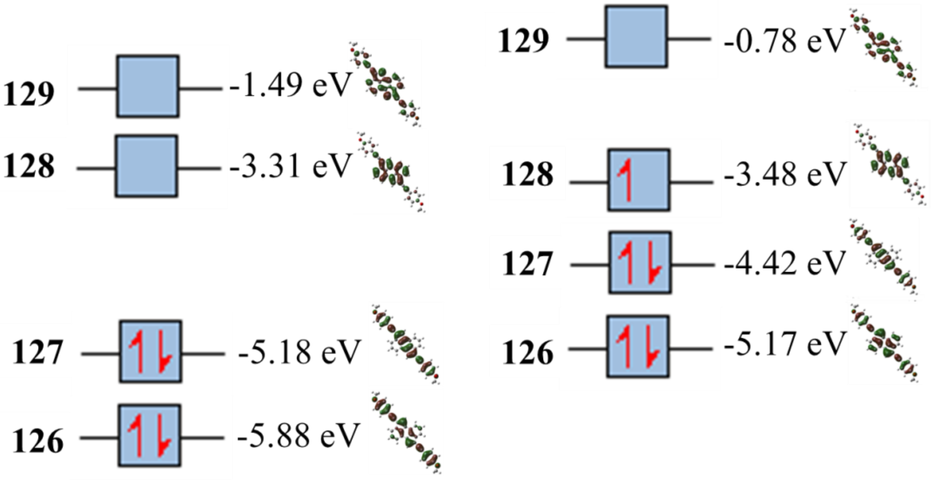

Figure 3. Contour plots and energy levels of neutral (charge= 0, left) and the reduced (charge= -1, right) state of **1** in THF calculated using B3LYP/6-311G(d,p).

The neutral state of **1** has an even number of electrons filling up to molecular orbital (MO) 127. When **1** is reduced to **1**$^-$, not only does the extra electron go into the LUMO (MO128) of the neutral species, but the energies of each MO also differentiate. Specifically, upon reduction (**1** to **1**$^-$), the energy of MO127 increased while MO128 decreased. This shows that the presence of an electron in LUMO lowers its energy. Therefore, the reduced form of a sample when characterized using cyclic voltammetry has different electronic behavior from the neutral form and should be accounted for in the prediction of the LUMO. In this work, we denote the MO128 in the -1 charged CP-PAH species as singly unoccupied MO (SUMO). We expect that calculations using 0 and -1 charged CP-PAH that closely represent the sample in experiment would provide more accurate LUMO and ΔE_{gap}. Indeed, the results in Table 4 demonstrated the improvement of the agreement with experiment.

Table 4. The energy values (in eV) obtained using the conventional and current method for predicting electronic properties of 1 and 2. All calculated were carried out in THF using B3LYP/6-311G(d,p).

	1			**2**		
Functional	HOMO	LUMO	ΔE_{gap}	HOMO	LUMO	ΔE_{gap}
Experiment[a]	-5.19	-3.64	1.55	-5.19	-3.62	1.57
Conventional[a]	-5.18	-3.31	1.88	-5.13	-3.31	1.82
Current	-5.18	-3.48	1.70	-5.13	-3.50	1.63

[a] Data taken from Ref. [15].

The conventional method, or protocol, provides a LUMO of **1** and **2** that is more than 0.30 eV higher than those of experiments and ΔE_{gap} more than 0.25 eV higher. The new method reduced the error of predicted LUMO energy to about 0.15 eV and ΔE_{gap} to about 0.10 eV. Therefore, the new method (protocol) provides a more accurate LUMO energy and ΔE_{gap} for **1** and **2** by closely reproducing the electrochemical experiments and significantly reducing the errors in comparison to those from the conventional method.

Finally, we mention that the shapes of orbital contours of the compound are not changed. Furthermore, there are differences between the optical and electrochemical HOMO-LUMO energy gap, ΔE_{gap}.[15] The difference is not simply experimental discrepancies but rather a reflection of the different processes that were being probed optically or electrochemically. The current protocol for ΔE_{gap} is to be compared with that from an electrochemical measurement. This indicates the prediction of the LUMO energy will be different depending on its application as an electron acceptor or donor. Thus, the LUMO energy predicted here is for use as electron acceptor.

3.1.3 The Best Functional for the Electronic Energies of CP-PAHs

Errors of predicted electronic properties of **1** and **2** using the six functionals with the conventional and new method are shown in Table 5. The electronic properties of **1** and **2** were calculated in the conventional protocol using only neutral molecules. Among the six functionals, CAM-B3LYP with the long range corrected exchange functional provided the worst predicted HOMO energy, LUMO energy, and ΔE_{gap} by using the conventional method. HOMO energy was significantly underestimated and LUMO energy was overestimated using CAM-B3LYP. PBE, TPSS, and HCTH, on the other hand, provided very similar predictions of HOMO energy, LUMO energy, and ΔE_{gap}. However, the ΔE_{gap} from PBE, TPSS, and HCTH calculations are almost half of the experimental value.

The new method obtained HOMO energy the same way as the conventional method. However, the LUMO energy was obtained from the compound in a -1 state, i.e. an extra electron was added. As expected, ΔE_{gap} from the new method is different from the conventional value. The results in Table 5 show an improvement in the predicted LUMO energy using B3LYP and CAM-B3LYP but not so using HSEH1PBE, PBE, TPSS, and HCTH. Nevertheless, predicted ΔE_{gap} using all six functionals was improved significantly except for ΔE_{gap} of **1** using HSEH1PBE.

The new method most accurately predicts the energies of HOMO and LUMO and ΔE_{gap} of **1** and **2** using B3LYP. Thus, in the calculations of CP-PAHs as electron acceptors, we adopted B3LYP and the new method for predicting HOMO energy, LUMO energy, and ΔE_{gap}.

Table 5. Errors of predicted HOMO, LUMO, and ΔE_{gap} of 1 and 2 with the errors in LUMO and ΔE_{gap} using conventional method shown in parentheses. The experimental values are also provided. All data are in eV.

	1			**2**		
Functional	HOMO	LUMO	ΔE_{gap}	HOMO	LUMO	ΔE_{gap}
Experiment[a]	-5.19	-3.64	1.55	-5.19	-3.62	1.57
B3LYP[*]	0.01	0.16	0.14	0.06	0.12	0.06
		(0.33)	(0.32)		(0.31)	(0.25)
CAMB3LYP	-1.24	-0.85	0.39	-1.12	-0.81	0.31
		(1.30)	(2.55)		(1.28)	(2.40)
HSEH1PBE	0.15	0.27	0.13	0.20	0.23	0.04
		(0.05)	(-0.10)		(0.01)	(-0.19)
PBE	0.60	0.55	-0.04	0.61	0.47	-0.14
		(-0.13)	(-0.73)		(-0.18)	(-0.79)
TPSS	0.64	0.61	-0.02	0.66	0.53	-0.12
		(-0.03)	(-0.66)		(-0.07)	(-0.73)
HCTH	0.53	0.51	-0.02	0.55	0.43	-0.12
		(-0.17)	(-0.70)		(-0.22)	(-0.76)

[a]data from experiment and conventional B3LYP method were taken from Ref. [15].

These different predictions using various functionals were partially reflected in the optimized geometries. As shown in Table 2, different functionals predict the bond length changes between neutral and negatively charged species differently. The differences in bond distances calculated using other functionals with respect to B3LYP are discernible. For example, in comparison to the B3LYP results, the bond lengths of **1** from CAM-B3LYP calculations are shorter and can be as much as 0.0169 Å. We found that 18 of the 22 C-C bond lengths of the cyclopenta[hi]aceanthrylene core of **1** are shorter. As expected, this decrease in bond length using CAM-B3LYP would correlate to an overestimation of the LUMO energy and ΔE_{gap}. It is, indeed, the case as the data shown in Table 5. HSEH1PBE also provided shorter bond lengths in comparison to B3LYP with the maximum decrease of 0.0064 Å, less drastic than CAM-B3LYP. All 22 C-C bond lengths of the cyclopenta[hi]aceanthrylene core decreased, but not as severe as those from CAM-B3LYP. PBE and TPSS both produced very similar results where 20 out of 22 C-C bonds in the aromatic core were shorter than those of B3LYP. HCTH produced a slightly different result in which 12 out of the 22 C-C bond lengths in the core were decreased in comparison to B3LYP.

3.1.4 The Best Functional for Absorption Spectra of CP-PAHs

Prediction of λ_{max} in absorption spectra of **1** and **2** was made using TD-B3LYP/6-311G (d,p)[15] with a difference from experiment found to be 135nm and 157 nm, respectively. This implies TD-B3LYP is not the best. Therefore, we evaluated five more functionals for their performances in predicting absorption spectra of CP-PAHs. The accuracy was measured mainly on how well they predict λ_{max}, which corresponds to the lowest excitation. Table 6 summarizes the errors of the predicted λ_{max} of **1** and **2** from all six functionals with respect to the experimental data.

Table 6. The calculated λ_{max} differences (in nm) with respect to the experimental values (in nm).

Functional	**Difference**	
	1	**2**
Experiment[a]	686	699
TD-B3LYP	139	163
TD-CAM-B3LYP	-65	-61
TD-HSEH1PBE	142	174
TD-PBE	374	481
TD-TPSS	325	421
TD-HCTH	348	450
B3LYP/TD-CAMB3LYP	-9	-13

[a] data were taken from Ref. [15].

Among the six functionals, CAM-B3LYP provides the best λ_{max}, which confirms the need for a long–ranged corrected exchange in TD-DFT calculations. Although the E_{XC} formalism for B3LYP and CAM-B3LYP in Table 1 is similar, i.e. using identical correlation energy but with different coefficients for the exact exchange energy components, B3LYP provides a good prediction of orbital energies and geometry and CAM-B3LYP provides absorption spectra better. As previously stated, geometries optimized using CAM-B3LYP have shorter bond distances compared to B3LYP optimized structures. These shorter bond lengths in CAM-B3LYP optimized geometry result in an overestimation of energies such as ΔE_{gap}, thus providing a smaller λ_{max} compared to B3LYP. CAM-B3LYP has been proven here to be a good functional for absorption spectra of **1** and **2** that are in good agreement with experiment. B3LYP provides good predicted geometry, but is not a good functional to use in calculation of absorption spectra of the systems with a charge transfer character. Combining the strengths of B3LYP and CAM-B3LYP can provide the best absorption λ_{max} of CP-PAHs such as **1** and **2**. Thus, the more accurate way of predicting absorption spectra of CP-PAHs is by using TD-CAM-B3LYP preceded by B3LYP structure optimization, which we denote here as B3LYP/TD-CAM-B3LYP method.

We note that several other groups have used the B3LYP/TD-CAM-B3LYP protocol to predict absorption spectra of different systems. Fitri *et al.* used it to study ten thiazolothiazole based dyes[70] and thienpyrazine based dyes that resulted in excitation energies, absorption and emission spectra that are in good agreement with experimets.[71] Kumar *et al.* studied a hydroxyl radical reaction with guanine in an aqueous environment using B3LYP/TD-CAM-B3LYP for absorption spectra calculation and their results are also in good agreement with experiments.[72] The use of TD-CAM-B3LYP in absorption spectra is preferred over TD-B3LYP because B3LYP is not appropriate to use for ion pair or species involving excited states with charge transfer character where transition energies are greatly underestimated. However, TD-CAM-B3LYP has been very successful in studying these mentioned systems.[54, 69, 72-74] In a similar way, the long range corrected exchange functional included in CAM-B3LYP is proven here to work better in the TD-DFT study of **1** and **2** in comparison with TD-B3LYP.

Predicted absorption spectra of **1** and **2** using the six functionals and the B3LYP/TD-CAM-B3LYP are plotted in Figure 4. These absorption spectra of **1** and **2** can be classified into three groups based on accuracy. Group 1 (solid and dashed red curves in Figure 4) is CAM-B3LYP that provides the shortest λ_{max} and the least error. Group 2 (green and dashed black curves in Figure 4) includes the two hybrid functionals, B3LYP and HSEH1PBE, with similar λ_{max} and errors between 100-200 nm. Group 3 (yellow, blue, and purple solid curves) includes the GGA and meta-GGA functionals, PBE, HCTH, and TPSS, that predicted similar λ_{max}, but with the longest wavelengths and thus the largest error. Similarities in the accuracy of functionals in the same group can be attributed to the similar theory behind its derivation (see Table 1). Furthermore, the current results show that exchange energy is most sensitive to the excitation energy. For example, B3LYP and CAM-B3LYP have the same expression of correlation energy (Table 1), they differ in exchange energy. Using the same optimized geometry, the absorption spectra produced from these functionals are very different.

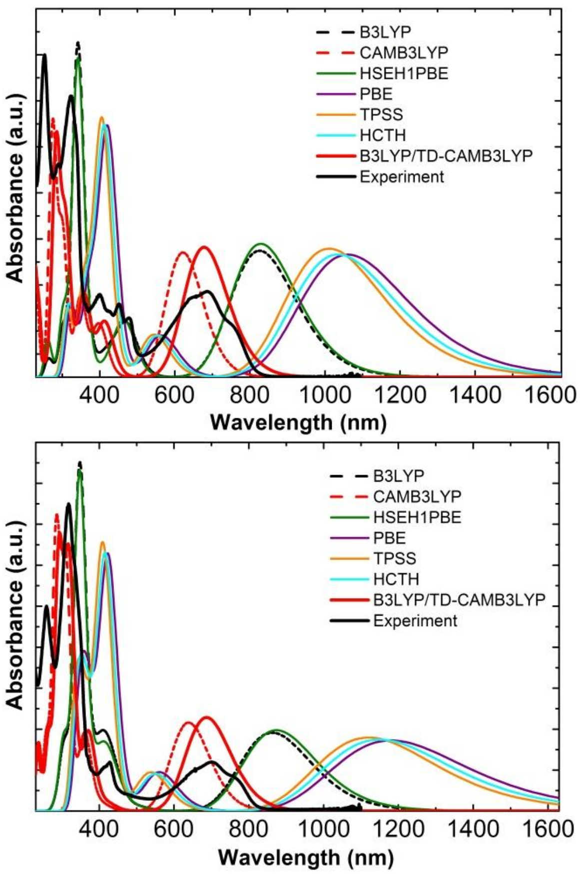

Figure 4. Experimental and calculated absorption spectra of **1** (top) and **2** (bottom).

3.2 Validation of Current Protocol for CP-PAHs

Results from **1** and **2** demonstrated that B3LYP should be used to calculate orbital energies and B3LYP/TD-CAM-B3LYP for absorption spectra of CP-PAHs. Specifically, the current protocol is to calculate HOMO energy using the neutral species and LUMO energy using the species with -1 state, i.e. anion. The TD-CAM-B3LYP calculations are used to calculate absorption spectra with B3LYP optimized geometries of neutral CP-PAHs.

Six more CP-PAHs were used to validate the current method for predicting electronic properties of **3-8**, whose structures are shown in Figure 1. The results of errors and MAEs for

HOMO, LUMO, ΔE_{gap}, and λ_{max} of all eight CP-PAHs are provided in Tables 7 and 8. For comparison purposes, we also included those using conventional method for LUMO and ΔE_{gap}. We mention here that the experimental absorption spectrum was not available for **8** excluding it in the calculation of MAE for λ_{max}.

Table 7. Errors and MAEs of HOMO energy, LUMO energy, and ΔE_{gap}, together with the corresponding experimental values. Data in parentheses are the errors using the conventional method.

Functional	**1**	**2**	**3**	**4**	**5**	**6**	**7**	**8**	**MAE**
				HOMO (eV)					
Experiment	-5.19^{15}	-5.19^{15}	-5.59^{15}	-5.36^{15}	-5.88^{75}	-6.06^{76}	-6.37^{76}	-6.16^{76}	
B3LYP	0.01	0.06	-0.15	-0.06	0.34	0.20	0.02	0.11	0.12
HSEH1PBE	0.15	0.61	0.02	0.07	0.47	0.32	0.10	0.23	0.19
CAMB3LYP	-1.24	-1.12	-1.43	-1.21	-0.81	0.32	-1.40	-1.20	1.09
PBE	0.60	0.61	0.49	0.46	0.83	0.86	0.65	0.76	0.66
TPSS	0.64	0.66	0.52	0.51	0.88	0.90	0.70	0.80	0.70
HCTH	0.53	0.55	0.42	0.41	0.76	0.80	0.59	0.70	0.60
				LUMO (eV)					
Experiment	-3.64^{15}	-3.62^{15}	-3.41^{15}	-3.45^{15}	-4.00^{75}	-3.48^{76}	-2.55^{76}	-3.35^{76}	
B3LYP	0.16	0.12	0.16	0.16	0.38	0.21	0.06	0.14	0.17
	(0.33)	(0.32)	(0.34)	(0.32)	(0.52)	(0.68)	(0.55)	(0.63)	(0.46)
HSEH1PBE	0.05	0.47	0.29	0.27	0.50	0.32	0.21	0.27	0.30
	(0.27)	(-0.01)	(0.05)	(0.02)	(0.24)	(0.39)	(0.28)	(0.35)	(0.17)
CAMB3LYP	-0.85	-0.81	-0.89	-0.81	-0.70	-0.80	-0.87	-0.80	0.82
	(1.30)	(1.28)	(1.39)	(1.35)	(1.52)	(1.76)	(1.69)	(1.74)	(1.50)
PBE	0.55	0.47	0.60	0.52	0.87	0.61	0.40	0.48	0.56
	(-0.13)	(-0.18)	(-0.24)	(-0.25)	(0.04)	(0.06)	(-0.11)	(0.01)	(0.13)
TPSS	0.61	0.53	0.65	0.58	0.91	0.66	0.47	0.55	0.62
	(-0.03)	(-0.07)	(-0.12)	(-0.13)	(0.15)	(0.20)	(0.03)	(0.15)	(0.11)
HCTH	0.51	0.43	0.57	0.49	0.82	0.57	0.39	0.45	0.53
	(-0.17)	(-0.22)	(-0.27)	(-0.28)	(-0.01)	(0.04)	(-0.12)	(-0.01)	(0.14)
				ΔE_{gap} (eV)					
Experiment	1.55^{15}	1.57^{15}	2.18^{15}	1.91^{15}	1.88^{75}	2.58^{76}	3.82^{76}	2.81^{76}	
B3LYP	0.14	0.06	0.31	0.22	0.05	0.01	0.08	0.03	0.11
	(0.32)	(0.25)	(0.49)	(0.38)	(0.18)	(0.48)	(0.57)	(0.52)	(0.40)
HSEH1PBE	0.13	-0.14	0.31	0.20	0.03	-0.01	0.11	0.03	0.11
	(-0.01)	(-0.79)	(0.06)	(-0.05)	(-0.23)	(0.07)	(0.18)	(0.12)	(0.13)
CAMB3LYP	0.39	0.31	0.54	0.41	0.11	1.43	0.53	0.39	0.47
	(2.55)	(2.40)	(2.82)	(2.56)	(2.32)	(-1.12)	(3.10)	(2.93)	(2.52)
PBE	-0.04	-0.14	0.11	0.06	-0.79	-0.80	-0.25	-0.28	0.15
	(-0.73)	(-0.79)	(-0.73)	(-0.71)	(0.04)	(-0.25)	(-0.77)	(-0.74)	(0.76)
TPSS	-0.02	-0.12	0.13	0.07	-0.73	-0.70	-0.22	-0.24	0.14
	(-0.66)	(-0.73)	(-0.64)	(-0.64)	(0.03)	(-0.24)	(-0.66)	(-0.65)	(0.68)
HCTH	-0.02	-0.12	0.14	0.08	-0.77	-0.77	-0.20	-0.25	0.14
	(-0.70)	(-0.76)	(-0.69)	(-0.68)	(0.05)	(-0.23)	(-0.71)	(-0.71)	(0.72)

Note: superscripts are the References from which the data were taken.

Table 8. Errors and MAEs of λ_{max}(nm) together with the corresponding experimental values.

Functional	1	2	3	4	5	6	7	MAE
Experimental	**686**[15]	**699**[15]	**548**[15]	**603**[15]	**568**[75]	**363**[77]	**286**[77-78]	
TD-B3LYP	139	164	47	61	129	153	63	108
TD-CAMB3LYP	-65	-61	-48	-53	-21	56	23	47
TD-HSEH1PBE	142	174	39	55	118	146	56	104
TD-PBE	374	481	165	200	262	275	104	266
TD-TPSS	325	421	132	167	229	247	94	231
TD-HCTH	348	450	149	184	249	265	98	249
B3LYP/TD-CAMB3LYP	-9	-13	-25	-29	29	70	30	29

Note: superscripts are the References from which the data were taken.

A comparison of MAEs from different functionals is also illustrated in Figure 5 for the HOMO energy, LUMO energy, ΔE_{gap}, and λ_{max}. It is clear from the current results that among the six functionals studied, B3LYP is the best in predicting HOMO energy with the smallest MAE of 0.12 eV.

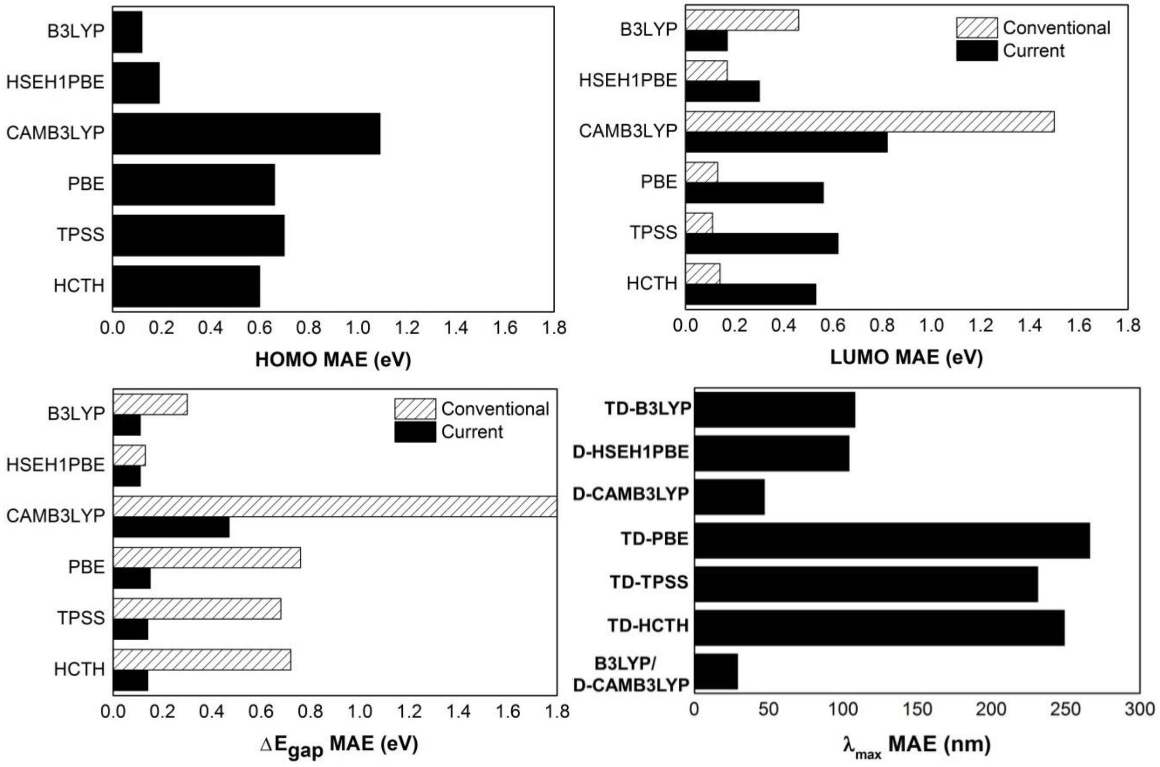

Figure 5. Mean Absolute Errors (MAEs) of predicted HOMO, LUMO, ΔE_{gap}, and λ_{max}.

Improved accuracy in LUMO energies using the current method was also observed using B3LYP and CAM-B3LYP, but higher MAEs were found using HSEH1PBE, PBE, TPSS, and HCTH. It is important to point out that the small error in ΔE_{gap} is largely due to the error cancellation of HOMO and LUMO energies. B3LYP prediction of LUMO energy using the current protocol is the most accurate method with a MAE of 0.17 eV. Furthermore, the current protocol provides an improvement over the conventional method by reducing the MAE by more than 50%.

A comparison of accuracy of ΔE_{gap} shows similar results as that of LUMO energy. The current method shows a significant improvement in ΔE_{gap} values using all six functionals. B3LYP and HSEH1PBE provided a similar accuracy with a MAE of 0.11 eV. An overall MAE for all three quantities, HOMO, LUMO, and ΔE_{gap}, was also calculated to determine the best functional. Among the six functionals, B3LYP predicted all three quantities the most accurate with MAE of 0.14 eV. This validates the use of B3LYP in the current method for accurately predicting HOMO, LUMO and ΔE_{gap}. The significant improvement in accuracy of LUMO and ΔE_{gap} of the eight CP-PAHs using the current method confirms its validity on accurately predicting electronic properties of CP-PAH systems.

Six other CP-PAHs shown in Figure 1 were employed to validate the choice of using B3LYP/TD-CAMB3LYP to calculate absorption spectra. In addition to the results provided in Table 8 and Figure 5, we also provide a detailed comparison of calculated spectra here (Figure 6). All the results confirm that the six functionals can be classified into three groups. Group 1 with CAM-B3LYP has predicted λ_{max} for all eight CP-PAHs with the shortest wavelength and the smallest MAE of 47 nm. Group 2 with B3LYP and HSEH1PBE has very similar accuracy with MAE of 108 nm and 104 nm, respectively, and both overestimated λ_{max} by more than 100 nm. Group 3 with PBE, TPSS, and HCTH overestimated λ_{max} with more than 200 nm.

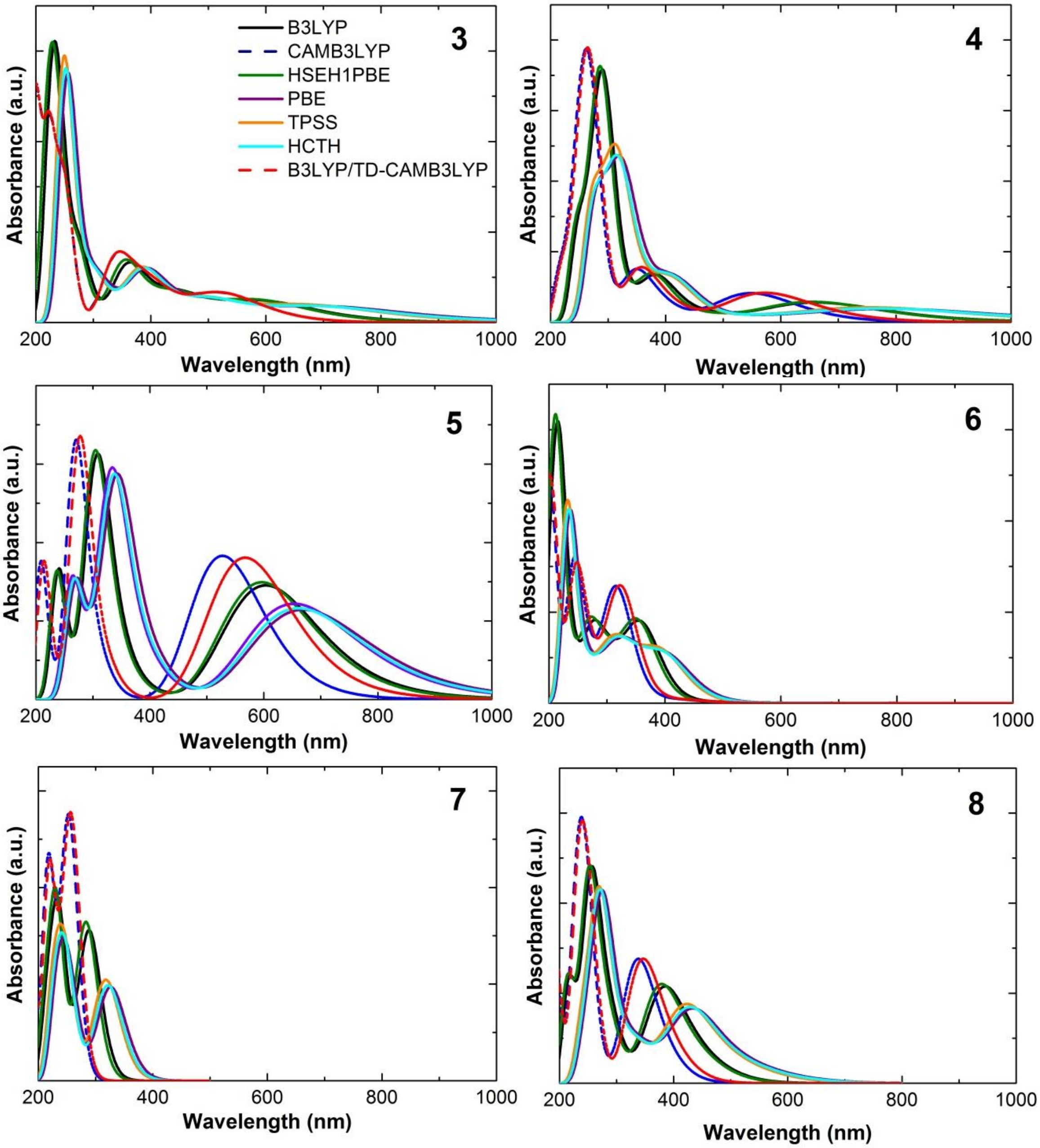

Figure 6. Absorption spectra of **3**- **8** (structures in Figure 1) calculated using six functionals.

The explanation of the trend in errors of λ_{max} can be made by comparing the orbital contours, which are summarized in Table 9. Among the eight CP-PAHs, we can group the compounds into three pairs, two pairs having similar cores, i.e. **1** & **3**, **2** & **4**, and the third pair, **6** &**7**, that can be used to illustrate the point to be made.

Table 9. HOMO and LUMO contours with the orbital energy (eV) of the eight CP-PAHs obtained from B3LYP calculations. The orbital energies in parentheses were from the corresponding anion (-1 state).

CP-PAH	HOMO	LUMO (neutral)
1	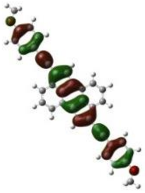 -5.18 (-4.42)	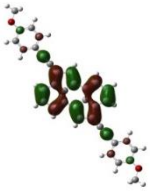 -3.31 (-3.48)
2	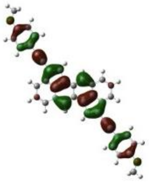 -5.13 (-4.42)	 3.31 (-3.50)
3	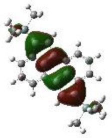 -5.74 (-4.68)	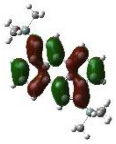 -3.07 (-3.25)
4	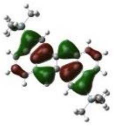 -5.42 (-4.57)	 -3.13 (-3.29)
5	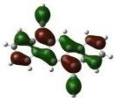 -5.54 (-4.77)	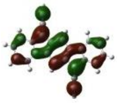 -3.48 (-3.62)
6	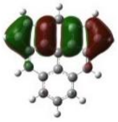 -5.86 (-5.05)	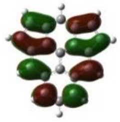 -2.80 (-3.27)
7	 -6.39 (-5.45)	 -2.00 (-2.49)
8	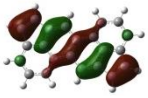 -6.05 (-5.30)	 -2.72 (-3.21)

The HOMO contours of **1** and **2** both have a distributed electron density stretched to the aryl substituent group. Upon excitation to LUMO, the electron density migrates to the center, thus providing less spatial overlap between HOMO and LUMO. On the other hand, **3** and **4** have shorter groups attached to the CP-PAH core, resulting in a greater spatial overlap between HOMO and LUMO. Thus, the error of λ_{max} of **3** and **4** is almost three times less than that of **1** and **2,** respectively. The same was observed in **6** and **7**, which are $C_{20}H_{10}$ isomers. A greater spatial overlap between HOMO and LUMO can be seen visually in **7** compared to **6,** thus with a smaller λ_{max} error. This has also been observed by Peach *et al.* for other systems where the less spatial overlap between HOMO and LUMO the greater the excitation energy or wavelength error.[53]

Among the six functionals, CAM-B3LYP is the best in predicting λ_{max} of CP-PAHs. However, by using a good predicted structure of CP-PAHs from B3LYP followed by TD-CAM-B3LYP calculation, the most accurate λ_{max} is obtained with the least MAE of 29 nm. This validates the use of B3LYP/TD-CAMB3LYP and provides the most accurate λ_{max}.

Finally, we note that our findings in the accuracy of these six functionals to predict HOMO, LUMO, ΔE_{gap}, and absorption spectra of CP-PAHs are similar to those found for other systems by several groups. A comparison of the results made by these groups and ours is provided in Table 10. Most studies give more emphasis to the prediction of ΔE_{gap} in comparison to those of HOMO and LUMO energies. Overall, based on ours and the studies from others, HSEH1PBE and CAM-B3LYP give the smallest for ΔE_{gap} and λ_{max}, respectively. However, the prediction by using B3LYP is the most accurate for electronic properties, including the HOMO and LUMO energies and ΔE_{gap}.

Table 10. Accuracy of the six functionals in predicting HOMO (eV), LUMO (eV), ΔE_{gap} (eV), and λ_{max}.

Functional	**Reference**	**Data Set**		**MAE**	**of**	
			HOMO	**LUMO**	ΔE_{gap}	λ_{max}
B3LYP	This work	8 CP-PAHs	0.12	0.17	0.11	108 nm
	Su *et al.*[51]	7 atoms and 5 molecules	0.37	0.25	0.59	
	Zhang *et al*[52]	27 molecules from H_2 to $C_{14}H_{10}$	3.10		1.63	
	Dev *et al.*[79]	3 TPA donor dyes – isolated				0.61 eV
	Le Bahers *et al.*[50]	11 semiconductors			0.56	
	Jacquemin *et al.*[80]	34 organic dyes				15 nm
	Wroblewski *et al.*[81]	4 diatomic molecules		0.24		
	Ernzerhof *et al.*[82]	38 atoms and molecules	0.17	0.11		
CAM-B3LYP	This work	8 CP-PAHs	1.09	0.82	0.47	47 nm
	Dev *et al.*[79]	3 TPA donor dyes – isolated				0.11 eV
	Peach *et al.*[54]	Triazene chromophores				0.11 eV
	Jacquemin *et al.*[80]	34 organic dyes				10 nm
	Rabilloud[83]	6 Ag clusters				0.08 eV
HSEH1PBE	This work	8 CP-PAHs	0.19	0.30	0.11	104 nm
	Le Bahers *et al.*[50]	11 semiconductors			0.21	
	Heyd *et al.*[84]	40 semiconductors			0.26	
	Guo *et al.*[60]	8 benzoic acid derivatives (neutral)				0.24 eV
PBE	This work	8 CP-PAHs	0.66	0.56	0.15	266 nm
	Zhang *et al.*[52]	27 molecules from H_2 to $C_{14}H_{10}$	4.33		0.73	
	Le Bahers *et al.*[50]	11 semiconductors			0.83	
	Heyd *et al.*[84]	40 semiconductors			1.13	
	Peach *et al.*[54]	Triazene chromophores				1.38 eV
	Jacquemin *et al.*[80]	34 organic dyes				33 nm
	Wroblewski *et al.*[81]	4 diatomic molecules		0.19		
	Ernzerhof *et al.*[82]	38 atoms and molecules	0.16	0.13		
	Tao *et al.*[64]	86 species for IP, 58 for EA	0.22	0.12		
TPSS	This work	8 CP-PAHs	0.70	0.62	0.14	231 nm
	Heyd *et al.*[84]	40 semiconductors			0.98	
	Jacquemin *et al.*[80]	34 organic dyes				29 nm
	Wroblewski *et al.*[81]	4 diatomic molecules		0.16		
	Tao *et al.*[64]	86 species for IP, 58 for EA	0.23	0.14		
HCTH	This work	8 CP-PAHs	0.60	0.53	0.14	249 nm
	Rushton *et al.*[85]	10 semiconductors			0.76	
	Wroblewski *et al.*[81]	4 diatomic molecules		0.26		

Note: superscript numbers are the References from which the data were taken.

3.3 CP-PAHs as Electron Acceptors

We have established a protocol to study CP-PAHs through the evaluation of six functionals using eight CP-PAHs. The current method or protocol for predicting HOMO energy, LUMO energy, and ΔE_{gap} of CP-PAHs is to use B3LYP. The HOMO energy is obtained from the neutral CP-PAH, while the LUMO energy is calculated from the corresponding anion with a -1 charge. ΔE_{gap} is then calculated by the difference between the HOMO and LUMO energies. The method for predicting absorption spectra of CP-PAHs is to use TD-CAM-B3LYP with B3LYP optimized geometries of neutral species.

The most essential quantities for electron acceptors are their HOMO and LUMO energy levels with respect to the donor materials. The first criterion of selecting acceptor is to align the HOMO and LUMO levels of acceptor candidates with the donor materials. The HOMO and LUMO levels of eight CP-PAHs being studied here are depicted in Figure 7 together with the HOMO and LUMO of P3HT.

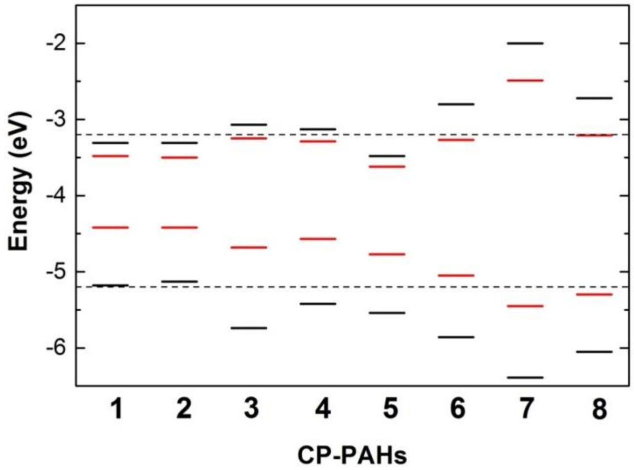

Figure 7. The HOMO and LUMO energies of **1**- **8** (structures see Figure 1) calculated using B3LYP. The dashed lines are the HOMO and LUMO energy of P3HT.[15] The black lines are the energies of neutral species and the red lines are the energies of the corresponding anion (with -1 charge).

Among eight CP-PAHs, six of them, **1**-**6** can accept electron from P3HT as their LUMO energies are lower than that of P3HT. The LUMO of **3** is about 0.2 eV lower than the LUMO of P3HT and the energy difference is slightly smaller than 0.3 eV, which is a threshold considered to be dynamically favorable for electron transfer.[86] However, the remaining five CP-PAHs have a LUMO that provides energy offset of greater than 0.3 eV of the LUMO of P3HT. More interestingly, after these CP-PAHs accept an electron from P3HT, their HOMO levels (red HOMOs in Figure 7) will simultaneously increase to facilitate the change. All six HOMOs are higher than that of P3HT, which implies that the electron occupying these HOMOs can be transferred to the newly emptied HOMO of P3HT, making these P3HT-CP-PAHs potential ambipolar materials.

Absorption spectra of the eight CP-PAHs are also plotted in Figure 8. The absorption wavelength of **1**, **2**, and **5** is extended to longer than 600 nm. The common feature of these compounds is its inclusion of an aryl substituent on each of the two 5-membered rings in these compounds.

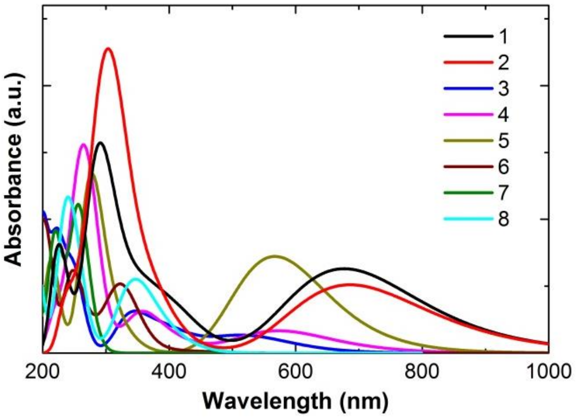

Figure 8. Absorption spectra of **1**-**8** obtained from the B3LYP/TD-CAM-B3LYP calculations.

In the development of more efficient small-molecule OPV materials, we recently proposed a donor-acceptor1-acceptor2 architecture and demonstrated that forming such a cascade architecture is superior to the traditional D-A architecture.[14] Inspired by this work, we set out here to look for acceptor pairs that can form cascade energy levels, ideally for both HOMO and LUMO so that they facilitate electron as well as hole transport. Upon inspection of the data set in Figure 7, we identified three pairs of acceptors: **6**-**1**, **6**-**2**, and **6**-**5** that fulfill the requirement as cascade acceptor pairs. Therefore, three set of materials including P3HT-**6-1**, P3HT-**6-2**, and P3HT-**6-5** form cascaded LUMOs as well as cascaded HOMOs. We note that the LUMO energy of **6** is about 0.30 eV lower than that of P3HT, which is a good match. From the energetics point of view, these materials may be ambipolar, which offers great potential for electron and hole transportation.

4. Conclusions

A protocol to accurately predict the electronic properties and absorption spectra of CP-PAHs as electron acceptors was developed and validated using eight CP-PAHs. Six functionals, B3LYP, CAM-B3LYP, HSEH1PBE, PBE, TPSS, and HCTH, were evaluated for their accuracy. Electronic properties of CP-PAHs, namely the HOMO, LUMO, and ΔE_{gap}, were predicted accurately using B3LYP. While the HOMO energy was obtained from the neutral species, the LUMO energy was obtained as the SUMO of the corresponding anion (-1 state). This new method of calculating LUMO energy for electron acceptors was proven to be more accurate than the conventional method that uses only the neutral model. More importantly, the new method reflects the state of compounds in the electrochemical experiment. MAEs of predicted HOMO energy, LUMO energy, and ΔE_{gap} using the new method are 0.12 eV, 0.17 eV, and 0.11 eV, respectively, based on a data set of eight CP-PAHs. Absorption spectra of CP-PAHs, on the other hand, were accurately predicted using B3LYP/TD-CAMB3LYP. The calculated λ_{max} using this method yields an MAE of 29 nm, which is significantly smaller than those using B3LYP.

From comparison of the LUMO and HOMO energy levels of eight CP-PAHs with the widely used donor material P3HT in OPVs, it was found that six of these eight CP-PAHs can accept electrons from P3HT, thus indicating they can be used as electron acceptors of P3HT. Moreover, three pairs of CP-PAHs were identified to form a P3HT-acceptor1-acceptor2 architecture, which may significantly improve the cell efficiency. Finally, the protocol being developed in this work offers us an opportunity to perform calculations to establish a highly accurate data set (an acceptor library) for selection of better electron acceptors for OPVs.

■ AUTHOR INFORMATION

Corresponding Author

*Email: lwang@chem.siu.edu. Tel: 618-453-6476.

Notes

The authors declare no competing financial interest.

■ ACKNOWLEDGEMENT

This work has been supported by Illinois Clean Coal Institute (ICCI/IDCEO-14/ER-7). Part of this work has also been supported by a National Science Foundation CAREER grant (CHE-1352431).

■ REFERENCES

1. Mariotti, N.; Bonomo, M.; Fagiolari, L.; Barbero, N.; Gerbaldi, C.; Bella, F.; Barolo, C., Recent Advances in Eco-Friendly and Cost-Effective Materials Towards Sustainable Dye-Sensitized Solar Cells. *Green Chem.* **2020**, *22*, 7168-7218.

2. Wang, X.; Zhao, B.; Kan, W.; Xie, Y.; Pan, K., Review on Low-Cost Counter Electrode Materials for Dye-Sensitized Solar Cells: Effective Strategy to Improve Photovoltaic Performance. *Adv. Mater.* **2022**, *9*, 2101229.
3. He, S.; Lan, Z.; Zhang, B.; Gao, Y.; Shang, L.; Yue, G.; Chen, S.; Shen, Z.; Tan, F.; Wu, J., Holistically Optimizing Charge Carrier Dynamics Enables High-Performance Dye-Sensitized Solar Cells and Photodetectors. *ACS Appl. Mater. Interfaces* **2022**, *14*, 43576-43585.
4. Ge, F.; Xu, F.; Gong, K.; Liu, D.; Li, W.; Wang, L.; Zhou, X., Sensitizers Designed toward Efficient Intramolecular Charge Separation for p-Type Dye-Sensitized Solar Cells. *Dyes Pigm.* **2022**, *200*, 110127.
5. Xu, F.; Gong, K.; Liu, D.; Wang, L.; Li, W.; Zhou, X., Enhancing Photocurrent of Dye-Sensitized Solar Cells through Solvent Modulating Aggregation of Dyes. *Solar Energy* **2022**, *240*, 157-167.
6. Koteshwar, D.; Prasanthkumar, S.; Singh, S. P.; Chowdhury, T. H.; Bedja, I.; Islam, A.; Giribabu, L., Effects of Methoxy Group(S) on D-π-A Porphyrin Based Dsscs: Efficiency Enhanced by Co-Sensitization. *Mater. Chem. Front.* **2022**, *6*, 580-592.
7. Sun, H.; Li, P.; Liu, D.; Wang, T.; Li, W.; Hu, W.; Wang, L.; Zhou, X., Tuning Photophysical Properties Via Alkoxyl Groups in Charge-Separated Triphenylamine Sensitizers for Dye-Sensitized Solar Cells. *J. Photochem. Photobiol. A: Chem.* **2019**, *368*, 223-241.
8. Venkatesan, S.; Hsua, T.-H.; Wong, X.-W.; Teng, H.; Lee, Y.-L., Tandem Dye-Sensitized Solar Cells with Efficiencies Surpassing 33% under Dim-Light Conditions. *Chem. Eng. J.* **2022**, *446*, 137349.
9. Sun, H.; Liu, D.; Wang, T.; Lu, T.; Li, W.; Ren, S.; Hu, W.; Wang, L.; Zhou, X., Enhanced Internal Quantum Efficiency in Dye-Sensitized Solar Cells: Effect of Long-Lived Charge-Separated State of Sensitizers. *ACS Appl. Mater. Interfaces* **2017**, *9*, 9880.
10. Agrawal, A.; Siddiqui, S. A.; Soni, A.; Sharma, G. D., Advancements, Frontiers and Analysis of Metal Oxide Semiconductor, Dye, Electrolyte and Counter Electrode of Dye Sensitized Solar Cell. *Solar Energy* **2022**, *233*, 378-407.
11. Sun, H.; Liu, D.; Wang, T.; Li, P.; Bridgmohan, C. N.; Li, W.; Lu, T.; Hu, W.; Wang, L.; Zhou, X., Charged-Separated Sensitizers with Enhanced Intramolecular Charge Transfer for Dye-Sensitized Solar Cells: Insight from Structure-Performance Relationship. *Org. Electronics* **2018**, *61*, 35-45.
12. Wang, T.; Sun, H.; Zhang, L.; Colley, N. D.; Bridgmohan, C. N.; Liu, D.; Hu, W.; Li, W.; Zhou, X.; Wang, L., Effect of Photo-Induced Charge Separated State Lifetimes in Donor-Acceptor1-Acceptor2 Organic Ambipolar Semiconductors on Their Photovoltaic Performances. *Dyes Pigm.* **2017**, *139*, 601.
13. Cnops, K.; Rand, B. P.; Cheynes, D.; Verreet, B.; Empl, M. A.; Heremans, P., 8.4% Efficient Fullerene-Free Organic Solar Cells Exploiting Long-Range Exciton Energy Transfer. *Nature Commun.* **2014**, *5*, 3406.

14. Wang, T.; Weerasinghe, K. C.; Liu, D.; Li, W.; Yan, X.; Zhou, X.; Wang, L., Ambipolar Organic Semiconductors with Cascades of Energy Levels for Generating Long-Lived Charge Separated States: A Donor–Acceptor1–Acceptor2 Architectural Triarylamine Dye. *J. Mater. Chem. C* **2014**, *2*, 5466-5470.
15. Wood, J.D.; Jellison, J. L.; Finke, A.D.; Wang, L.; Plunkett, K.N., Electron Acceptors Based on Functionalizable Cyclopenta[hi] Aceanthrylenes and Dicyclopenta[de,mn]Tetracenes. *J. Am. Chem. Soc.* **2012**, *134*, 15783-15789.
16. Wang, T.; Weerasinghe, K. C.; Ubaldo, P. C.; Liu, D.; Li, W.; Zhou, X.; Wang, L., Tuning Electron-Hole Distance of the Excitons in Organic Molecules using Functional Groups *Chem. Phys. Lett.* **2015**, *618*, 142-146.
17. Chen, C.-C.; Chang, W.-H.; Yoshimura, K.; Ohya, K.; You, J.; Gao, J.; Hong, Z.; Yang, Y., An Efficient Triple-Junction Polymer Solar Cell Having a Power Conversion Efficiency Exceeding 11%. **2014**, *26*, 5670-5677.
18. Jo, J.; Pouliot, J.-R.; Wynands, D.; Collins, S. D.; Kim, J. Y.; Nguyen, T. L.; Woo, H. Y.; Sun, Y.; Leclerc, M.; Heeger, A. J., Enhanced Efficiency of Single and Tandem Organic Solar Cells Incorporating a Diketopyrrolopyrrole-Based Low-Bandgap Polymer by Utilizing Combined ZnO/Polyelectrolyte Electron-Transport Layers. *Adv. Mater.* **2013**, *25*, 4783-4788.
19. Yuan, B.; Zhuang, J.; Kirmess, K. M.; Bridgmohan, C. N.; Whalley, A. C.; Wang, L.; Plunkett, K. N., Pentaleno[1,2-a:4,5′]Diacenaphthylenes: Uniquely Stabilized Pentalene Derivatives. *J. Org. Chem.* **2016**, *81*, 8312.
20. Nagaraju, N.; Kushavah, D.; Kumar, S.; Ray, R.; Gambhir, D.; Ghosh, S.; Pal, S. K., Through Structural Isomerism: Positional Effect of Alkyne Functionality on Molecular Optical Properties. *Phys. Chem. Chem. Phys.* **2022**, *24*, 3303-3311.
21. Kandregula, G. R.; Mandal, S.; Mirle, C.; Ramanujam, K., A Computational Approach on Engineering Short Spacer for Carbazole-Based Dyes for Dye-Sensitized Solar Cells. *J. Photochem. Photobiol. A: Chem.* **2021**, *419*, 113447.
22. Tarsang, R.; Promarak, V.; Sudyoadsuk, T.; Namuangruk, S.; Jungsuttiwong, S., Tuning the Electron Donating Ability in the Triphenylamine-Based D-π-A Architecture for Highly Efficient Dye-Sensitized Solar Cells. *J. Photochem. Photobio. A: Chem.* **2014**, *273*, 8.
23. Yang, J.; Liu, D.; Lu, T.; Sun, H.; Li, W.; Testoff, T. T.; Zhou, X.; Wang, L., Effects of Heterocyclic Ring and Amino-Ethyl-Amino Group on the Electronic and Photophysical Properties of a Triphenylamine-Pyrimidine Dye. *Int. J. Quantum. Chem.* **2020**, *120*, e26355.
24. Xu, F.; Testoff, T. T.; Wang, L.; Zhou, X., Cause, Regulation and Utilization of Dye Aggregation in Dye-Sensitized Solar Cells. *Molecules* **2020**, *25*, 4478.
25. Fan, X.; Wu, Z.; Wang, L.; Wang, C., Exploring the Origin of High Dechlorination Activity in Polar Materials $M_2B_5O_9Cl$ (M= Ca, Sr, Ba, Pb) with Built-in Electric Field. *Chem. Mater.* **2017**, *29*, 639.
26. Eastham, N. D., et al., Small Molecule Acceptor and Polymer Donor Crystallinity and Aggregation Effects on Microstructure Templating: Understanding Photovoltaic Response in Fullerene-Free Solar Cells. *Chem. Mater.* **2017**, *29*, 4432.

27. Lee, J.-W.; Jeong, D.; Kim, D. J.; Phan, T. N.-L.; Park, J. S.; Kim, T.-S.; Kim, B. J., Flexible-Spacer Incorporated Polymer Donors Enable Superior Blend Miscibility for High-Performance and Mechanically-Robust Polymer Solar Cells. *Energy Environ. Sci.* **2021**, *14*, 4067-4076.
28. Fagiolari, L.; Varaia, E.; Mariotti, N.; Bonomo, M.; Barolo, C.; Bella, F., Poly(3,4-Ethylenedioxythiophene) in Dye-Sensitized Solar Cells: Toward Solid-State and Platinum-Free Photovoltaics. *Adv. Sust. Systems* **2021**, *5*, 2100025.
29. Wang, T.; Weerasinghe, K. C.; Sun, H.; Hu, X.; Lu, T.; Liu, D.; Hu, W.; Li, W.; Zhou, X.; Wang, L., Effect of Triplet State on the Lifetime of Charge Separation in Ambipolar D-A_1-A_2 Organic Semiconductors. *J. Phys. Chem. C* **2016**, *120*, 11338.
30. Wang, T., et al., Enhancing Photoinduced Charge Separation through Donor Moiety in Donor-Accepter Organic Semiconductors. *J. Phys. Chem. C* **2016**, *120*, 25263-25275.
31. Wang, T.; Sun, H.; Lu, T.; Weerasinghe, K. C.; Liu, D.; Hu, W.; Zhou, X.; Wang, L.; Li, W.; Liu, L., Tuning Photophysical Properties and Electronic Energy Levels of 1-Aminoanthraquinone Derivatives by Introducing n-Ethyl Substituent. *J. Mol. Struct.* **2016**, *1116*, 256-263.
32. Lu, T.; Sun, H.; Colley, N. D.; Bridgmohan, C. N.; Liu, D.; Li, W.; Hu, W.; Zhou, X.; Wang, T.; Wang, L., Tuning the Donors to Control the Lifetimes of Charge-Separated States in Triazine-Based Donor-Acceptor Systems. *Dyes Pigm.* **2017**, *136*, 404.
33. Zhao, C., et al., Synthesis and Characterization of Triphenylamine Modified Azobenzene Dyes. *Dye Pigm.* **2017**, *137*, 256-264.
34. Zhou, X.; Liu, D.; Wang, T.; Hu, X.; Guo, J.; Weerasinghe, K. C.; Wang, L.; Li, W., Synthesis and Photophysical Studies of Triazine-Linked Porphyrin-Perylene Bismide Dyad with Long-Lived Perylene Triplet State. *J. Photochem. Photobiol. A: Chem.* **2014**, *274*, 57.
35. Liao, X. X.; Wang, T. S.; Wang, J. Z.; Zheng, J. C.; Wang, C. R.; Yam, V. W. W., Optoelectronic Properties of a Fullerene Derivative Containing Adamantane Group. *ACS Appl. Mater. Interfaces* **2013**, *5*, 9579-9584.
36. Cheng, Y. J. L., M. H.; Chang, C. Y.; Kao, W. S.; Wu, C. E.; Hsu, C. S., Di(4-Methylphenyl)Methano-C_{60} Bis-Adduct for Efficient and Stable Organic Photovoltaics with Enhanced Open Circuit Voltage. *Chem. Mater.* **2011**, *23*, 4056-4062.
37. Walkup, L. L.; Weerasinghe, K. C.; Tao, M.; Zhou, X.; Zhang, M.; Liu, D.; Wang, L., Importance of Dynamics in Electron Excitation and Transfer of Organic Dyes. *J. Phys. Chem. C* **2010**, *114*, 19521-19528.
38. Li, C. Z.; Chueh, C. C.; Yip, H. L.; Zou, J.; Chen, W. C.; Jen, A. K. Y., Evaluation of Structure-Property Relationships of Solution-Processible Fullerene Acceptors and Their N-Channel Field-Effect Transistor Performance. *J. Mater. Chem.* **2012**, *22*, 14976-14981.
39. Meng, X. Y.; Zhang, W. Q.; Tan, Z. A.; Li, Y. F.; Ma, Y. H.; Wang, T. S.; Jiang, L.; Shu, C. Y.; Wang C. R., Highly Efficient and Thermally Stable Polymer Solar Cells with Dihydronaphthyl-Based [70] Fullerene Bisadduct Derivative as the Acceptor. *Adv. Funct. Mater*. **2012**, *22*, 2187-2193.

40. Xie, Q. A., F.; Echegoyen, L., Electrochemically-Reversible, Single Electron Oxidation of C_{60} and C_{70}. *J. Am. Chem. Soc.* **1993**, *115*, 9818-9819.
41. Reed, C. A.; Bolskar, R. D., Discrete Fulleride Anions and Fullerenium Cations. *Chem. Rev.* **2000**, *100*, 1075-1120.
42. Gooijer, C.; Kozin, I.; Velthorst, N. H.; Sarobe, M.; Jenneskens, L. W.; Vlietstra, E. J., The Spholskii Fluorescence Spectrum of Cyclopenta[cd] Pyrene. Novel Evidence for Anomalous S2 Emission. *Spectrochim. Acta. Part A* **1998**, *54*, 1443-1449.
43. Plummer, B. F.; Singleton, S. F., An Analysis of the Electronic States of Aceanthrylene. *J. Phys. Chem.* **1990**, *94*, 7363-7366.
44. Sarobe, M.; Flink, S.; Jenneskens, L. W.; Van Poecke, B. L. A.; Zwikker, J. W., Cyclopent[fg]Acepyrylene, Cyclopent[jk]Acepyrylene and Cyclopent[mn]Acepyrylene: Novel $C_{20}H_{10}$ Cyclopenta-Fused Polycyclic Aromatic Hydrocarbons. *J. Chem. Soc., Chem. Commun.* **1995**, *23*, 2415-2416.
45. Paranthaman, S.; Hong, K.; Kim, J.; Kim, D. E.; Kim, T. K., Density Functional Theory Assessment of Molecular Structures and Energies of Neutral and Anionic Al_n (n=2-10) Clusters. *J. Phys. Chem. A* **2013**, *117*, 9293-9303.
46. Becke, A. D., Density-Functional Thermochemistry. III. The Role of Exact Exchange. *J. Chem. Phys.* **1993**, *98*, 5648-5652.
47. Lee, C., Yang, W., Parr, R. G., Development of the Colle-Salvetti Correlation-Energy Formula into a Functional of the Electron Density. *Phys. Rev. B* **1988**, *37*, 785-789.
48. Cohen, A. J.; Mori-Sanchez, P.; Yang, W. T., Challenges for Density Functional Theory. *Chem. Rev.* **2012**, *112*, 289-320.
49. Zhao, Y.; Truhlar, D. G., Density Functionals with Broad Applicability in Chemistry. *Acc. Chem. Res.* **2008**, *41*, 157-167.
50. Le Bahers, T.; Rerat, M.; Sautet, P., Semiconductors Used in Photovoltaic and Photocatalytic Devices: Assessing Fundamental Properties from DFT. *J. Phys. Chem. C* **2014**, *118*, 5997-6008.
51. Su, N. Q.; Yang, W. T.; Mori-Sanchez, P.; Xu, X., Fractional Charge Behavior and Band Gap Predictions with the Xyg3 Type of Doubly Hybrid Density Functionals. *J. Phys. Chem. A* **2014**, *118*, 9201-9211.
52. Zhang, G.; Musgrave, C. B., Comparison of DFT Methods for Molecular Orbital Eigenvalue Calculations. *J. Phys. Chem. A* **2007**, *111*, 1554-1561.
53. Peach, M. J. G.; Benfield, P.; Helgaker, T.; Tozer, D. J., Excitation Energies in DFT: An Evaluation and Diagnostic Test. *J. Chem. Phys.* **2008**, *128*.
54. Peach, M. J. G.; Le Sueur, C. R.; Ruud, K.; Guillaume, M.; Tozer, D. J., TDDFT Diagnostic Testing and Functional Assessment for Triazene Chromophores. *J. Chem. Phys.* **2009**, *11*, 4465-4470.
55. Dev, P.; Agrawal, S.; English, N. J., Determining the Appropriate Exchange-Correlation Functional for Time-Dependent Density Functional Theory Studies of Charge-Transfer Excitations in Organic Dyes. *J. Chem. Phys.* **2012**, *136*, 224301-1 to 11.

56. Plotner, J.; Tozer, D. J.; Dreuw, A., Dependence of Excited State Potential Energy Surfaces on the Spatial Overlap of the Kohn-Sham Orbitals and the Amount of Nonlocal Hartree-Fock Exchange in Time-Dependent Density Functional Theory. *J. Chem. Theory Comput.* **2010**, *6*, 2315-2324.
57. Yang, J.; Wang, X.; Yim, W. L.; Wang, Q., Computational Study on the Intramolecular Charge Separation of D-A-π-A Organic Sensitizers with Different Linker Groups. *J. Phys. Chem. C* **2015**, *119*, 26355-26361.
58. Kuritz, N.; Stein, T.; Baer, R.; Kronik, L., Charge-Transfer-Like π(->)π* Excitations in Time-Dependent Density Functional Theory: A Conundrum and Its Solution. *J. Chem. Theory Comput.* **2011**, *7*, 2408-2415.
59. Rabilloud, F., Assessment of the Performance of Long-Range-Corrected Density Functionals for Calculating the Absorption Spectra of Silver Clusters. *J. Phys. Chem. A* **2013**, *117*, 4267-4278.
60. Guo, H. B.; He, F.; Gu, B. H.; Liang, L. Y.; Smith, J. C., Time-Dependent Density Functional Theory Assessment of UV Absorption of Benzoic Acid Derivatives. *J. Phys. Chem. A* **2012**, *116*, 11870-11879.
61. Heyd, J.; Scuseria, G. E., Efficient Hybrid Functional Calculations in Solids: Assessment of the Heyd Scuseria Ernzerhof Screened Coulomb Hybrid Functional. *J. Chem. Phys.* **2004**, *121*, 1187-1192.
62. Heyd, J.; Scuseria, G. E., Assessment and Validation of a Screened Coulumb Hybrid Density Functional. *J. Chem. Phys.* **2004**, *120*, 7274-7280.
63. Perdew, J. P., Burke, K., Ernzerhof, M., Generalized Gradient Approximation Made Simple. *Phys. Rev. Lett.* **1996**, *77*, 3865-3868.
64. Tao, J., Perdew, J. P., Staroverov, V. N., Scuseria, G. E., , Climbing the Density Functional Ladder: Nonemperical Meta-Generalized Gradient Approximation Designed for Solecules and Solid. *Phys. Rev. Lett.* **2003**, *91*, 146401-1-4.
65. Hamprecht, F. A., Cohen, A. J., Tozer, D. J., Handy, N. C., Development and Assessment of New Exchange-Correlation Functionals. *J. Chem. Phys.* **1998**, *109*, 6264-6271.
66. Frisch, M. J., et al. *Gaussian 09*, Gaussian, Inc.: Wallingford CT, 2009.
67. Hudson, G. A.; Cheng, L.; Yu, J.; Yan, Y.; Dyer, D. J.; McCarrol, M. E.; L. Wang, Computational Studies on Response and Binding Selectivity of Fluoresence Sensors. *J. Phys. Chem. B* **2010**, *114*, 870.
68. McCarroll, M. E.; Shi, Y.; Harris, S.; Puli, S.; Kimaru, I.; Xu, R.; Wang, L.; Dyer, D. J., Computational Prediction and Experimental Evaluation of a Photoinduced Electron-Transfer Sensor. *J. Phys. Chem. B* **2006**, *110*, 22991.
69. Yanai, T.; Tew, D. P.; Handy, N. C., A New Hybrid Exchange-Correlation Functional Using Coulomb Attenuating Method (Cam-B3LYP). *Chem. Phys. Lett.* **2004**, *393*, 51-57.
70. Fitri, A. T. B., A.; Benzakour, M.; Mcharfi, M.; Sfaira, M.; Hamidi, M.; Bouachrine, M., Theoretical Investigation of New Thiazolothiazole-Based D-π-A Organic Dyes for Efficient Dssc. *Spectrochimica Acta Part A: Mol. Biomol. Spectrosc.* **2014**, *124*, 646-654.

71. Bourass, M. F., A.; Benjelloun, A. T.; Benzakour, M.; Mcharfi, M.; Hamidi, M.; Serein-Spirau, F.; Jarrosson, T.; Lere-Porte, J. P.; Sotiropoulos, J. M.; Bouacharine, M., DFT and TDDFT Investigations of New Thienpyrazine-Based Dyes for Solar Cells: Effects of Electron Donor Groups. *Der Pharma Chemica* **2013**, *5*, 144-153.
72. Kumar, A. P. V. S., MD., Hydroxy Rarical (OH) Reaction with Guanine in an Aqueous Environment: A DFT Study. *J. Phys. Chem. B* **2011**, *115*, 15129-15137.
73. Dreuw, A. H.-G., M., Single-Reference Ab Initio Methods for the Calculation of Excited States of Large Molecules. *Chem. Rev.* **2005**, *105*, 4009-4037.
74. Dreuw, A. W., J. L.; Head-Gordon, M., Long-Range Charge-Transfer Excited States in Time Dependent Density Functional Theory Require Non-Local Exchange. *J. Chem. Phys.* **2003**, *119*, 2943-2946.
75. Chase, D.T.; Fix, A.G.; Rose, B.D.; Weber, C.D.; Nobusue, S.; Stockwell, C.E.; Zakharov, L. N.; Lonergan, M.C.; Haley, M.M., Electron-Accepting 6,12-Diethynylindeno[1,2-b]Fluorenes: Synthesis, Crystal Structures, and Photophysical Properties. *Angew. Chem. Int. Ed.* **2011**, *50*, 11103-11106.
76. Koper, C.; Sarobe, M.; Jenneskens, L. W., Redox Properties of Non-Alternant Cyclopenta-Fused Polycyclic Aromatic Hydrocarbons: The Effect of Peripheral Pentagon Annelation. *Phys. Chem. Chem. Phys.* **2004**, *6*, 319-327.
77. Lafleur, A. L.; Howard, J. B.; Taghizadeh, K.; Plummer, E. F.; Scott, L. T.; Necula, A.; Swallow, K. C., Identification of $C_{20}H_{10}$ Dicyclopentapyrenes in Flames: Correlation with Corannulene and Fullerene Formation. *J. Phys. Chem.* **1996**, *100*, 17421-17428.
78. Seiders, T. J.; Elliott, E. L.; Grube, G. H.; Siegel, J. S., Synthesis of Corannulene and Alkyl Derivatives of Corannulene. *J. Am. Chem. Soc.* **1999**, *121*, 7804-7813.
79. Dev, P.; Agrawal, S.; English, N. J., Functional Assessment for Predicting Charge-Transfer Excitations of Dyes in Complexed State: A Study of Triphenylamine-Donor Dyes on Titania for Dye-Sensitized Solar Cells. *J. Phys. Chem. A* **2013**, *117*, 2114-2124.
80. Jacquemin, D.; Perpete, E. A.; Vydrov, O. A.; Scuseria, G. E.; Adamo, C., Assessment of Long Range Corrected Functionals Performance for n-> π* Transitions in Organic Dyes. *J. Chem. Phys.* **2007**, *127*, 094102.
81. Wroblewski, T.; Hubisz, K.; Antonowicz, J., Theoretical Study of Electron Affinities for Selected Diatomic Molecules. *Optica Applicata* **2010**, *40*, 601-608.
82. Ernzerhof, M.; Scuseria, G. E., Assessment of the Pbe Exchange-Correlation Functional. *J. Chem. Phys.* **1999**, *110*, 5029-5036.
83. Rabilloud, F., Assessment of the Performance of Long-Range-Corrected Density Functionals for Calculating the Absorption Spectra of Silver Clusters. *J. Phys. Chem. A* **2013**, *117*, 4267-4278.
84. Heyd, J.; Peralta, J. E.; Scuseria, G. E., Energy Band Gaps and Lattice Parameters Evaluated with HSE Screnned Hybrid Functional. *J. Chem. Phys.* **2005**, *123*, 174101-1-8.

85. Rushton, P. P.; Clark, S. J.; Tozer, D. J., Density-Functional Calculations of Semiconductor Properties Using a Semiempirical Exchange-Correlation Functional. *Phys. Rev. B* **2001**, *63*, 4.
86. Scharber, M. C.; Mühlbacher, D.; Koppe, M.; Denk, P.; Waldauf, C.; Heeger, A. J.; Brabec, C. J., Design Rules for Donors in Bulk-Heterojunction Solar Cells—Towards 10% Energy-Conversion Efficiency. *Adv. Mater.* **2006**, *18*, 789-794.

Table of Contents (TOC) Graphics Image